Water Research 101 (2016) 597–605

Contents lists available at ScienceDirect

Water Research

journal homepage: www.elsevier.com/locate/watres

Enhanced simultaneous PEC eradication of bacteria and antibiotics by facilely fabricated high-activity {001} facets TiO_2 mounted onto TiO_2 nanotubular photoanode

Guiying Li [a, b], Xin Nie [a], Jiangyao Chen [b], Po Keung Wong [d], Taicheng An [a, b, *], Hiromi Yamashita [e], Huijun Zhao [c, **]

[a] State Key Laboratory of Organic Geochemistry and Guangdong Key Laboratory of Environmental Protection and Resources Utilization, Guangzhou Institute of Geochemistry, Chinese Academy of Sciences, Guangzhou, 510640, China
[b] Institute of Environmental Health and Pollution Control, School of Environmental Science and Engineering, Guangdong University of Technology, Guangzhou, 510006, China
[c] Centre for Clean Environment and Energy, Griffith University, Gold Coast Campus, QLD, 4222, Australia
[d] School of Life Sciences, The Chinese University of Hong Kong, Shatin, NT, Hong Kong Special Administrative Region, China
[e] Division of Materials and Manufacturing Science, Graduate School of Engineering, Osaka University, 2-1 Yamadaoka, Suita, Osaka, 565-0871, Japan

ARTICLE INFO

Article history:
Received 23 March 2016
Received in revised form
1 June 2016
Accepted 1 June 2016
Available online 4 June 2016

Keywords:
TiO_2-based photoanode
{001} facets TiO_2
Photoelectrocatalysis
Bacterial inactivation
Ciprofloxacin degradation

ABSTRACT

Biohazards and coexisted antibiotics are two groups of emerging contaminants presented in various aquatic environments. They can pose serious threat to the ecosystem and human health. As a result, inactivation of biohazards, degradation of antibiotics, and simultaneous removal of them are highly desired. In this work, a novel photoanode with a hierarchical structured {001} facets exposed nano-size single crystals (NSC) TiO_2 top layer and a perpendicularly aligned TiO_2 nanotube array (NTA) bottom layer (NSC/NTA) was successfully fabricated. The morphology and facets of anatase TiO_2 nanoparticles covered on the top of NTA layer could be controlled by adjusting precalcination temperature and heating rate as the pure NTA was clamped with glasses. Appropriate recalcination can timely remove surface F from {001} facets, and the photocatalytic activity of the resultant photoanode was subsequently activated. NSC/NTA photoanode fabricated under 500 °C precalcination with 20 °C min^{-1} followed by 550 °C recalcination possessed highest photoelectrocatalytic efficiency to simultaneously remove bacteria and antibiotics. Results suggest that two-step calcination is necessary for fabrication of high photocatalytic activity NSC/NTA photoanode. The capability of simultaneous eradication of bacteria and antibiotics shows great potential for development of a versatile approach to effectively purify various wastewaters contaminated with complex pollutants.

1. Introduction

Biohazards are a kind of emerging contaminants (ECs) presented in various aquatic environments (Dobrowsky et al., 2014; Rizzo et al., 2013). These pathogenic microorganisms can cause outbreaks of various waterborne diseases, thus posing serious threat to the ecosystem and human health (de Man et al., 2014). Conventional water disinfection methods such as chlorination and UV irradation have been frequently proved to possess many drawbacks. For instance, the formation of toxic and potential carcinogenic disinfection byproducts is the main drawbacks of chlorine treatment (Acero et al., 2013). Chlorination and UV irradiation disinfection did not contribute to significant reduction of antibiotic resistant genes and antibiotic resistant bacteria (Munir et al., 2011). Besides, another group of ECs, antibiotics, often coexisted with biohazards in many wastewaters and even in drinking water (Almeida et al., 2014). Current evidence suggests that the widespread antibiotics have contributed to the propagation and spread of antibiotics resistant microorganisms (Baquero et al., 2008; Fletcher, 2015; Na et al., 2014), which compromise our

* Corresponding author. Institute of Environmental Health and Pollution Control, School of Environmental Science and Engineering, Guangdong University of Technology, Guangzhou, 510006, China.
** Corresponding author.
E-mail addresses: antc99@gdut.edu.cn (T. An), h.zhao@griffith.edu.au (H. Zhao).

http://dx.doi.org/10.1016/j.watres.2016.06.001
0043-1354/

ability to fight infections, and many common procedures carry greater risks (Mather, 2014). Nevertheless, the removal of these antibiotics is not so efficient using the conventional water treatment technologies since they were not designed to remove these ECs. Consequently, extensive efforts have been made to ensure the safety of water and improve the quality of water through enhanced treatment strategies and technologies to effectively remove microbial pathogens and coexisted antibiotics.

Semiconductor (especially nano-sizsed TiO_2) photocatalysis has been proved as one of the most promising new technologies to treat wastewater containing a wide array of organic contaminants and biohazards due to its superior photocatalytic oxidation ability, high photocorrosion resistance, nontoxic and inexpensive properties (An et al., 2015; Gao et al., 2012; Li et al. 2011, 2015; Marugan et al., 2010; Sun et al., 2014). For anatase TiO_2, single crystal anatase TiO_2 with exposed {001} facets possesses higher photocatalytic activity than other facets (Stefanov et al., 2016; Yang et al., 2008). In this regard, extensive research has since been devoted to synthesize TiO_2 crystals with exposed {001} facets. Yang et al. first successfully synthesized {001} facets dominated anatase TiO_2 single crystals using hydrofluoric acid (HF) as a capping and shape-controlling agent (Yang et al., 2008). This pioneering work provides a promising application prospect, such as in solar cells, photocatalyst for hydrogen production from water and degradation of organic pollutants (Liu et al., 2010; Yang et al., 2011; Zhang et al., 2010).

However, in many conventional applications, TiO_2 was almost exclusively carried out in particle suspension system, which is not beneficial to the electron transport and the recycling of the used photocatalysts. Conversely, the immobilization of nanoparticle TiO_2 enables the application of electrochemical (photoelectrocatalytic (PEC)) techniques to enhance the photoefficiency due to the effectively suppressed photoelectron and hole recombination (Zhao et al., 2004). Nevertheless, for PEC applications, the overall performance is determined not only by the individual photocatalyst particle performance but also the connectivity among particles (Benkstein et al., 2003; Yu et al., 2009); and a poor connectivity among TiO_2 particles increases electron transport resistance, intensifies the recombination and hence reduces photocatalytic efficiency (Benkstein et al., 2003; Yu et al., 2009). Recently, highly ordered TiO_2 nanotube array (NTA) directly synthesized by anodizing the Ti foil has attracted considerable attentions due to its unique chemical and physical properties (Grimes et al., 2009; Schmuki et al., 2011). Compared with a nanoparticulate film, such a NTA can effectively improve the charge transport rate as well as slow the recombination time of photoelectron and hole because of its perpendicularly aligned nanotubular architecture (Paulose et al., 2006; Zhu et al., 2007). Nevertheless, the PEC efficiency of such NTA is determined by the cross-section areas of the nanotube walls (Zhang et al., 2008), meaning that the hollow parts of nanotubes occupy valuable surface area but are inactive.

In this regard, to overcome these drawbacks and utilize the aforementioned advantages, that is, the high reactivity of {001} facets exposed nano-size single crystals and superior electron transport properties of NTA, fabrication of the composite photocatalysts with both components would be a possible way to enhance the pollutants removal efficiency of TiO_2-based photocatalyst. However, works about the TiO_2 NTA with exposed {001} facets are quite limited so far. One paper just fabricated similar kind of catalyst without any further application (Alivov and Fan, 2009), and another paper synthesized similar kind of catalyst to photocatalytically degradation of ordinary organics (Liao et al., 2013). As for PEC approach to remove pollutants, its application in bacterial inactivation and antibiotics degradation is the least exploited with only a few scattered reports (Butterfield et al., 1997; Cho et al., 2011; Daghrir et al., 2013; Liu et al., 2012), and most of researches on the PEC bacterial inactivation were previously carried out by our research group (An et al., 2016; Li et al., 2013; Nie et al., 2014a; Sun et al., 2016, Sun et al. 2014). Nevertheless, the PEC inactivation of biohazards, degradation of antibiotics, and simultaneous removal of them has not been previously attempted on this catalyst.

Herein, a novel TiO_2 based photoanode with a hierarchical structured {001} facets exposed nano-size single crystals (NSC) top layer and perpendicularly aligned nanotube array bottom layer (NSC/NTA) was successfully synthesized using a facile anodization-precalcination-recalcination approach. The effects of various prepared parameters, including the calcination temperature and heating rate, on the structure, morphology and photocatalytic activity of the resultant composite photoanodes were systematically investigated in detail. *Escherichia coli* and ciprofloxacin in water were chosen as the model biohazards and antibiotics to evaluate the PEC activity of prepared composite photoanodes.

2. Experimental section

2.1. Synthesis of the composite photoanode

In a typical process, highly oriented NTA was prepared by the potentiostatic anodization method in a two-electrode electrochemical cell (Fig. S1) at room temperature (~22 °C) according to our previous work (Nie et al., 2013). Rectangle Ti foil (1.5 × 10 cm, 99.6% purity, 0.16 mm thickness) was used as the substrate for NTA fabrication. During the synthesis process, ultrasonically cleaned Ti foil was used as an anode and same size Pt foil as cathode. The distance of two electrodes was fixed at 2 cm. A mixture solution containing 50 mL ethylene glycol, 0.5 M glacial HAc, 10 wt% H_2O, and 0.2 M NH_4F was used as an electrolyte. Ti foils were pre-anodized for 4 h at 30 V, and the produced films were cleaned by sonication in deionized water for 30 min, then pre-anodized Ti foils were further anodized at 30 V for 24 h.

The as-synthesized TiO_2 NTA films were washed with deionized water, clamped with two pieces of glasses, and then calcined in a muffle furnace at 300–550 °C for 2 h with a heating rate of 2–30 °C min^{-1} in air (precalcination), which was further calcined for another 3 h at 500–650 °C with a heating rate of 2 °C min^{-1} after the removal of glasses (recalcination).

2.2. Characterizations

2.2.1. General characterizations

The crystal phase composition and crystallinity, surface morphologies, as well as the elemental composition were characterized and the detail procedures are provided in Supporting Information.

2.2.2. Photoeletrochemical characterizations

The photoelectrochemical characterizations were carried out using a three-electrode system with a quartz window for UV illumination (Nie et al., 2014b). The composite photoanode, a Pt foil, and a saturated Ag/AgCl were employed as a working, counter electrode, and reference electrode, respectively. A microelectrochemical system (μECS) (USB2.0, PLAB, Changchun Institute of Applied Chemistry, China) powered and controlled by a laptop was used for the application of potential bias, the current signal recording and data processing in photoelectrochemical experiments. A UV-LED (NCCU033 (T), Nichia Corporation) with a wavelength of 365 nm and light intensity of 27 mW cm^{-2} was used as light source, and 0.2 M $NaNO_3$ aqueous solution was used as electrolyte.

2.3. Photocatalytic activity test

2.3.1. Inactivation of bacteria

E. coli K-12 (The Coli Genetic Stock Center at Yale University, USA) was chosen as the model bacterium to evaluate the inactivation efficiency of the as-prepared samples. The PEC inactivation of bacteria were conducted under constant applied potential of +1.0 V in a 50 mL quartz reactor in a three-electrode cell with the composite photoanode, a Pt foil, and a saturated Ag/AgCl were employed as a working, counter electrode, and reference electrode, respectively. The bacteria were cultured in nutrient broth growth medium at 37 °C for 16 h with shaking and then successively washed with sterilized water via the centrifugation. The bacterial cell concentration was adjusted to a final cell density of 10^7 colony-forming units per mL (cfu mL^{-1}) with 0.20 M $NaNO_3$ solution. Before each experiment, the reactor was washed several times to remove the residual organics which generated from decomposed bacteria, and all glassware and samples were sterilized by autoclaving at 120 °C for 15 min. The reaction temperature was kept at approximately 25 °C and the reaction solution was stirred with a magnetic stirrer throughout the experiment. For the PEC experiment, a +1.0 V of constant applied potential and 27 mW cm^{-2} of UV-LED array illumination were used. Photocatalytic (PC) and electrolytic (EC) inactivation experiments were also conducted under identical experimental conditions as PEC experiments, except the electrochemical system was disconnected and the light was switched off, respectively. In a typical inactivation experiment, 50 mL solution containing 10^7 cfu mL^{-1} *E. coli* was added into reactor. At different time intervals, approximately 1.5 mL inactivation solution was collected for further analysis of final bacterial survivability by diluting with sterilized saline solution and spreading 0.1 mL of the diluted sample uniformly on nutrient agar plates (3 plate repeats per sample). The plates were incubated at 37 °C for 16 h, the colonies were enumerated, and the initial number of bacteria was calculated. The *E. coli* inactivation data displayed in this work were the average values obtained from experiments replicated in triplicate.

During PEC inactivation process, field emission scanning electron microscope (FESEM) was used to observe the destruction process of *E. coli* cells. The SEM sample preparation procedure was similar to our previous work (Sun et al., 2014).

2.3.2. Degradation of antibiotics

Ciprofloxacin (>98% purity, Sigma–Aldrich), an antibiotic used to treat a number of bacterial infections and has been detected in different waters (Michael et al., 2013), was chosen as the model antibiotics to evaluate degradation efficiency of the as-prepared samples. The PEC, PC, and EC degradation of ciprofloxacin were carried out in the identical reactor and conditions as bacterial inactivation. The detailed degradation experiment procedures and the analysis are provided in Supporting Information.

3. Results and discussion

3.1. Characterization

3.1.1. Morphological and phase compositional properties of prepared photoanodes

A series of experiments was performed under different conditions (precalcination temperature, heating rate, and recalcination temperature) to understand the mechanism of the NSC/NTA photoanodes formation. The detailed description of morphological and phase compositional properties of NSC/NTA photoanodes as well as the images are provided in Supporting Information and in Figs. S2–S6. An optimized NSC/NTA photoanode was achieved as follows: the optimized TiO_2 NTA was firstly synthesized using potentiostatic anodization method (Nie et al., 2013); then the as-synthesized TiO_2 NTA were clamped with two pieces of glasses, and calcined in a muffle furnace at 500 °C for 2 h with a heating rate of 20 °C min^{-1} in air (precalcination) followed by recalcination at 550 °C with heating rate of 2 °C min^{-1} for 3 h after the removal of glasses.

As Fig. 1a shows, both characteristic peaks of anatase TiO_2 and titanium were observed from the XRD pattern of optimized photoanode. Specifically, peaks at $2\theta = 25.3°$, 48.0°, and 54.0° were attributed to the (101), (200), and (105) planes of anatase TiO_2, respectively (An et al., 2008; Liu et al., 2009c; Nie et al., 2013), while the peaks of Ti can also be indexed to $2\theta = 38.3°$ (002), 40.1° (101), 53.0° (102), 62.9° (110), 70.6° (103) and 76.2° (112) owing to the Bragg reflection of Ti foil in the sample.

Fig. 1b and c shows the SEM images of the optimized synthesis NSC/NTA photoanode. The highly ordered NTA layer (approximately 1.8 μm height) was directly grown onto Ti foil, and nano-size TiO_2 nanoparticle layer (approximately 1.2 μm thickness) fully dispersed onto the NTA layer (Fig. 1b), suggesting that the opening ends of partial TiO_2 nanotubes were transformed to nanoparticles when some of HF molecules in the nanotubes were volatilized into air at 500 °C calcination temperature under the semiclosed circumstance (Alivov and Fan, 2009). The dispersed upper layer of TiO_2 nanoparticles are cubic shape TiO_2 particles with average diameter of ~500 nm (Fig. 1c), and the two flat and square mirror-like surfaces can be ascribed to {001} facets of anatase TiO_2 crystal according to reference (Liu et al., 2009b).

The NSC/NTA photoanode prepared under the optimized condition was also characterized by transmission electron microscope (TEM). For NTA at bottom layer (Fig. 1d), the corresponding selected-area electron diffraction (SAED) pattern recorded from the circled area (upper-left inset in Fig. 1d) indicated a best fit to polycrystalline anatase (Zhang et al., 2011a). The corresponding high-resolution TEM (HRTEM) image (lower-left inset in Fig. 1d) showed that the lattice fringes spacing of 0.352 nm were assigned to {101} planes of anatase TiO_2. For the cube at top layer (Fig. 1e), the corresponding SAED pattern recorded from the circled area confirmed that the crystalline was single crystal with exposed {001} facet, indicating that the NTA opening ends were transformed from polycrystalline to single crystal. HRTEM image directly showed that the lattice fringes spacing was 0.235 nm, corresponding to {001} planes of anatase TiO_2 (An et al., 2012). That is, TiO_2 photoanode with a hierarchical structured {001} facets exposed nano-size single crystals top layer and a perpendicularly aligned NTA bottom layer was successfully fabricated.

The morphology and composition of photoanode could be controlled by adjusting precalcination temperature and heating rate (Figs. S3 and S4). According to reference (Nie et al., 2013), the formation of NTA photoanodes by electrochemical anodization of pure Ti was due to that HF served as a pore opening reagent. The consumed HF can be supplemented by the combination of F^- and H^+ generated from the dissociation of F source and acid, and HF concentration is maintained at constant levels in the electrolyte. In this study, during the precalcination process, the residual HF vaporized and moved to the opening ends of NTA directly facing the glass, where highly concentrated HF was obtained as the glass covered on the NTA film. Whereas, the NTA on the other side of the sample still aligned on Ti foil retained its nanotube array morphology. With further progress of precalcination, the opening ends of NTA shrank and collapsed due to that the HF adsorbed NTA surface was not energetically favorable at high temperatures. Simultaneously, the dissociative adsorption of HF dramatically reduced the surface energy of {001} facets, which facilitated the {001} facets growth. This resulted in the conversion of top TiO_2

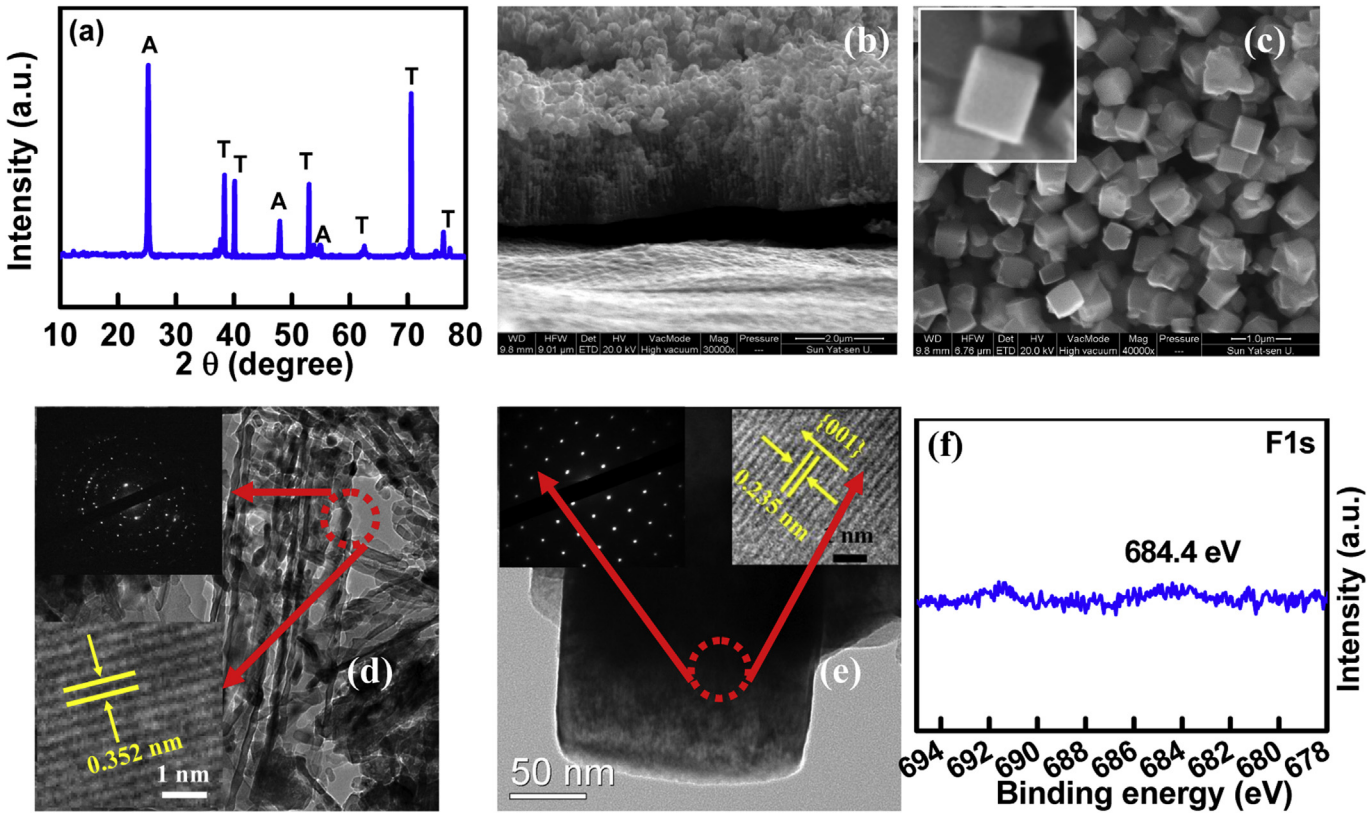

Fig. 1. (a) XRD pattern; (b) cross-sectional structure SEM image; (c) surface morphology SEM image; (d) cross section of TiO_2 nanotubes TEM image; (e) individual nanoparticles TEM image; and (f) XPS spectra of the composite photoanode precalcined at 500 °C with heating rate of 20 °C min^{-1} followed by 550 °C recalcination with heating rate of 2 °C min^{-1} for another 3 h (A: Anatase; T: Titanium).

from tubular shape to cube, and the dominant crystal facet was accordingly transformed from {101} to {001} facets based on previous report (Zhang et al., 2011b). As such, the cubic TiO_2 particles with exposed single-crystal {001} facets could be obtained after the densification and rearrangement of TiO_2 crystal. As known, the synthesized anatase TiO_2 is often dominated by {101} facets due to its low surface energy (0.44 J m^{-2}) because the {001} facets with a higher surface energy (0.90 J m^{-2}) can be rapidly diminished during the crystal growth (Yang et al., 2008). Therefore, to guarantee the transformation of {101} facets to {001} facets, and to stabilize higher surface energy {001} facets, sufficient HF at the opening ends of NTA directly facing the glass was a prerequisite (Alivov and Fan, 2009), which could be controlled by adding HAc during anodization, optimum precalcination temperature and heating rate.

More importantly, the recalcination temperature could also affect the morphology and composition of the photoanode. Fig. S5 shows SEM images of the photoanodes (after removal of glasses) recalcined at different temperatures with heating rate of 2 °C min^{-1} after precalcination at 500 °C with 20 °C min^{-1} heating rates. The description of morphology change of the photoanodes under various recalcination temperatures is provided in the Supporting Information. It can be found that the optimized recalcination temperature was 550 °C, which resulted in the formation of high-quality anatase TiO_2 cubic particles with mirror-like plane {001} facets. However, higher temperature (e.g. 650 °C) would lead to a seriously erosion of {001} facets (Fig. S5) with the transformation of anatase to rutile (Fig. S2). As reported, the anatase-to-rutile phase transformation prefer to occurring at higher temperatures (Jarosz et al., 2015). The eroded {001} facets were due to the HF etching/dissolution effect at high recalcination temperature (Zhang et al., 2011a). In addition, high recalcination temperature would lead to the break of surface Ti—F bond and subsequent to the volatilization of F (Liu et al., 2009a). This is because the surface F species played an important roles in the formation of high energy facets (Lai et al., 2012). Comparatively, the surface lattice F species was slowly removed at lower recalcination temperature, which will not lead to the destruction of {001} facets.

To clarify this issue, the presence of F element on the prepared photoanode was also characterized by X-ray photoelectron spectroscopy (XPS). As known, the centroid of F1s peak at 684.4 eV in samples corresponds to the typical value for surface Ti—F species (Gordon et al., 2012; Liao et al., 2013), but it almost could not be found under the optimized condition (Fig. 1f). This suggests that there is no or very limited surface Ti—F species existed under this condition. Nevertheless, high characteristic peak of F element was clearly observed for the photoanodes prepared without recalcination or recalcination temperature below 550 °C (Fig. S6), indicating the existence of F element on the photoanode surface. This is due to that, covered by two pieces of glasses, too much of F was concentrated in the semiclosed environment, and subsequently formed Ti—F species on the photoanode surface during the first run calcination process. This further proved that the existence of Ti—F bonding can greatly reduce the surface free energy of high energy {001} facets of anatase TiO_2, leading to the formation of single crystal with exposed {001} facets. Further, after removal of glasses, too low recalcination temperature still could not remove surface Ti—F species, but high recalcination temperature (≥550 °C) led to the break of surface Ti—F bond and subsequently to the volatilization of F (Liu et al., 2009a).

Based on the above results, a possible growth mechanism of the TiO_2-based NSC/NTA photoanode can be proposed (Fig. 2). First, highly ordered TiO_2 NTA was synthesized using an anodizing method from Ti foil as reported in our previous work (Nie et al., 2013). Second, after clamped with two pieces of glasses, the opening ends of TiO_2 NTA directly contacted with the glass transformed from anatase into {001} facets exposed nano-size single crystals TiO_2 by volatilized HF molecules during precalcination. This is due to that there exists some residual electrolyte (mixture of ethylene glycol, HAc, and NH_4F) in the nanotubes, two pieces of glasses can build a semi-closed circumstance to block the rapid evaporation of residual electrolyte during precalcination (Alivov and Fan, 2009), and the concentrated HF was obtained. The dissociative adsorption of HF at the opening ends of TiO_2 NTA dramatically reduced surface energy of {001} facets, which facilitated the {001} facets growth. Finally, after remove the covered glasses, appropriate recalcination can completely drive out the electrolyte residuals and effectively remove surface F element from {001} facets to improve photocatalytic activity of the resultant photoanode.

3.1.2. Photoeletrochemical analysis

The transient photocurrent density-time responses of resultant photoanodes were also analyzed. As Fig. S7 shows, except pure NTA and photoanode recalcined at 650 °C, the highest steady-state photocurrent density was obtained by the photoanode precalcined at 500 °C with heating rate of 20 °C min^{-1} followed by recalcined at 550 °C. The significantly high photocurrent density indicates efficient separation of photogenerated electrons and holes, and then high photocatalytic activity. However, lower photocurrent density was observed for the photoanodes precalcined below (or over) 500 °C. The reason might be the partially dispersed TiO_2 nanoparticle layer onto the NTA layer (or obtained film easily peeling off from Ti substrate), leading to poor connectivity among TiO_2 particles (or hinder of the charge transport to substrate) and hence reduced photocatalytic efficiency (Benkstein et al., 2003; Yu et al., 2009). It is worth noting that the steady-state photocurrent density of pure NTA calcined without glass coverage was extremely high, which is due to that directly grown perpendicularly aligned nanotube arrays onto the conducting substrate can facilitate electron transport and will increase photoefficiency (Zhang et al., 2008). In addition, although the obtained film can easily peel off from Ti substrate, high photocurrent density was also achieved for the photoanode recalcined at 650 °C, which is due to high content of rutile in this photoanode. The bandgap energy of rutile TiO_2 (3.0 eV) is slightly lower than that of anatase TiO_2 (3.2 eV), resulting in higher photocurrent. Similar results were also reported previously (Yu and Wang, 2010).

3.2. Inactivation of E. coli

Fig. S8 shows the direct photolysis, EC, PC and PEC inactivation of *E. coli* by the composite photoanode obtained under the optimized condition. Within 60 min, the bacterial population remained unchanged under only UV light irradiation or 1.0 V potential bias, and only 0.3 log *E. coli* was inactivated during PC process. In contrast, bacteria were completely inactivated after 45 min of PEC treatment, since the application of appropriate potential bias to photoanode can timely remove the photogenerated electrons and prolong the lifetime of photoholes. This is due to that, besides the production of high concentration of reactive species (RSs) served as bactericides, the holes could also directly inactivate bacteria (Li et al., 2011, 2013).

PEC inactivation of *E. coli* using photoanodes fabricated under various conditions was also carried out. Fig. 3a shows bactericidal performance of the photoanodes precalcined at different temperatures before 550 °C recalcination. For photoanode precalcined at 300 °C, only 3.5-log *E. coli* was inactivated within 60 min, since TiO_2 nanoparticle layer only partially dispersed onto NTA layer (Fig. S3) and the electron transport was not so smoothly. The bactericidal performance improved significantly and all bacteria were inactivated within 60 and 45 min by photoanodes precalcinated at 400 and 500 °C, respectively. This is due to the full coverage of TiO_2 nanoparticles onto NTA surface under these conditions, which facilitate electron transport and will increase the photoefficiency. Furthermore, the top layer is the TiO_2 nanoparticles with exposed single-crystal {001} facets for the photoanode precalcinated at 500 °C, meaning higher photocatalytic activity (Yang et al., 2008). However, the bactericidal performance decreased as the photoanode precalcined increased to 550 °C (bacteria were fully inactivated within 60 min), due to the decreased {001} faceted surface and the abscission of anodization layer (Fig. S3). In addition, although time needed to fully inactivate bacteria is the same (45 min) for pure NTA and photoanode precalcined at 500 °C, the inactivation efficiencies of the composite photoanode were much higher within shorter reaction time. This revealed that the highly reactive {001} facets possessed high photocatalytic activity to inactivate bacteria, although the steady-state photocurrent density

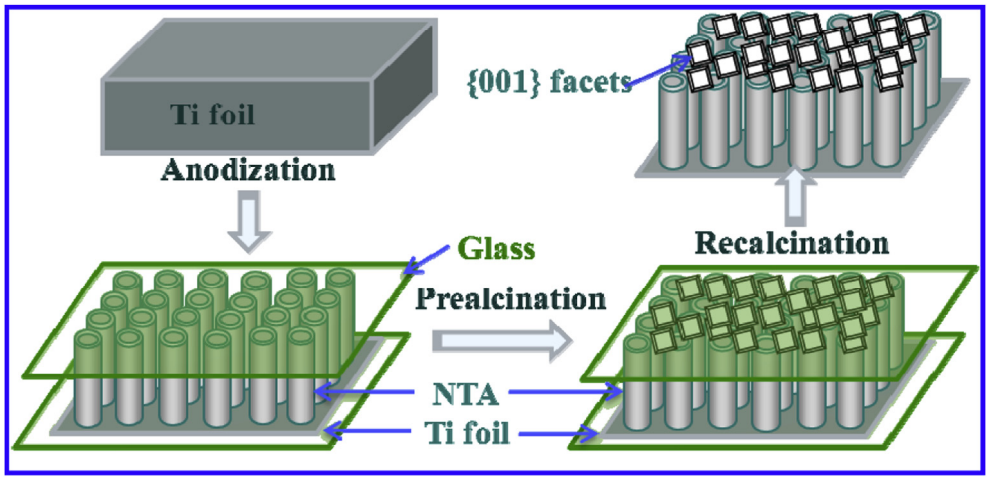

Fig. 2. Schematic diagram of the formation mechanism of NSC/NTA photoanode.

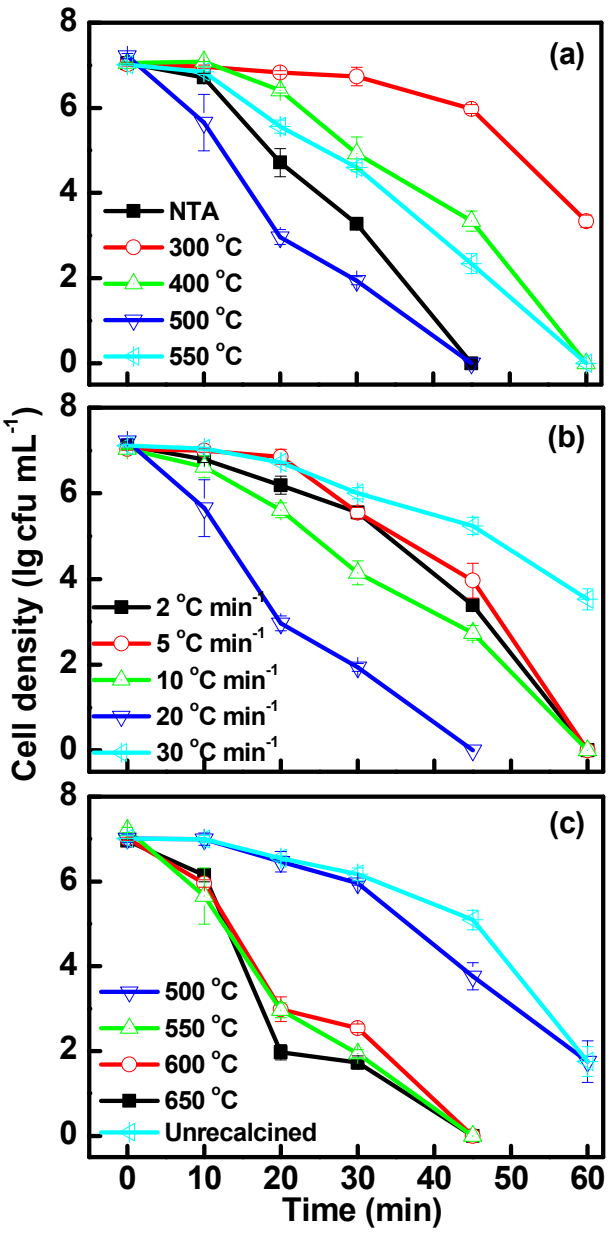

Fig. 3. The photoelectrocatalytic inactivation curves of *E. coli* by the composite photoanodes (a) calcined at different precalcination temperatures (heating rate: 20 °C min^{-1}; recalcination temperature: 550 °C); (b) calcined with different heating rates (precalcination temperature: 500 °C; recalcination temperature: 550 °C); (c) recalcined at different temperature after precalcination temperature of 500 °C with 20 °C min^{-1}. (NTA: pure TiO_2 nanotube array).

of pure NTA was the highest (Fig. S7).

Fig. 3b shows PEC inactivation of bacteria by photoanodes prepared at various heating rates. As shown, bacteria could be fully inactivated within 60 min by the photoanodes precalcined with the heating rates ranging from 2 to 10 °C min^{-1}, indicating that lower heating rates will not greatly influence PEC bactericidal performance of resultant photoanodes. As the heating rate further increased to 20 °C min^{-1}, the highest PEC bactericidal activity was achieved using the resultant photoanode (10^7 cfu mL^{-1} bacteria could be completely inactivated within 45 min), due to that bottom NTA layer surface was fully covered with highly reactive {001} facets. Nevertheless, further increasing heating rate to 30 °C min^{-1} led to a dramatic decrease of PEC bactericidal activity, by which only approximately 3.5-log reduction of bacteria was achieved within 60 min. This could be ascribed to the agglomeration of TiO_2 nanoparticles, abscission of anodization layer, and the decrease of {001} facets (Fig. S4e).

Furthermore, bacteria inactivation was also investigated by the photoanodes recalcined at different temperatures after 500 °C precalcination (Fig. 3c). For unrecalcined photoanode, the PEC bactericidal activity was the lowest as compared with recalcined photoanodes. This is due to that existence of surface Ti—F bonding in the {001} facets (Fig. S6), which is not favorable for the photocatalysis (Liao et al., 2013; Selloni, 2008). Comparatively, the time needed to inactivate 5.3-log bacteria was same for 500 °C recalcined photoanode, but its inactivation efficiencies were much higher within shorter reaction time. This is good agreement with our XPS and photoeletrochemical characterizations. With higher recalcination temperatures (≥550 °C), the surface lattice F species can effectively be removed (Fig. S6), leading to a significant improvement of PEC bactericidal activity of the resultant photoanodes, and all bacteria could be inactivated with 45 min. Although the bactericidal activity is slightly higher using photoanode recalcined at 650 °C, it is entire exposed reactive {001} facets were eroded (Fig. S5e). All these results indicate that recalcination is necessary for the formation of NSC/NTA photoanode with high PEC bactericidal performance.

From the results, it can be found that photoanode precalcined at 500 °C with heating rate of 20 °C min^{-1} followed by 550 °C recalcination with heating rate of 2 °C min^{-1} possesses highest PEC bactericidal activity. Therefore, FESEM was employed to examine the location and extent damages to bacterial cells during PEC treatment using optimized TiO_2 photoanode (Fig. 4). Before treatment, the bacteria have an intact cell structure and a well-preserved rod shape (Fig. 4a). Although the intact structure is still possessed, abnormal wavy surface could be observed after the cell subjecting to a 30-min PEC treatment (Fig. 4b). This suggests that some damages occurred to the cell membrane, which is supported by the dented cell due to the intracellular contents release. However, a longer PEC treatment of 60 min caused further morphological changes (Fig. 4c), and the complete leakage of intracellular contents occurred within 120 min (Fig. 4d), leading to a permanent bacterial inactivation.

3.3. Degradation of ciprofloxacin

Photolytic, EC, PC and PEC degradation of ciprofloxacin were also performed using photoanode prepared under optimized condition (Fig. S9). Similar with the EC bacterial inactivation, the ciprofloxacin concentration almost remain constant within 120 min. However, unlike bacteria, approximately 37% and 70% of ciprofloxacin could be degraded within 120 min under only UV light irradiation and PC process, respectively. Furthermore, the highest degradation efficiency was obtained during PEC process that approximately 94% of ciprofloxacin was eradicated within 120 min. These indicated that the resultant optimized photoanode can also effectively remove not only bacteria but also antibiotics during PEC process.

PEC degradation of ciprofloxacin was also conducted using photoanodes fabricated under various conditions. Using photoanodes precalcined at different temperatures before 550 °C recalcination (Fig. S10a), although the difference of the PEC degradation efficiency trend is not so obvious, the change trend is the same as the bacterial inactivation. That is, PEC degradation efficiencies increased first, peaked and then decreased with the increase of precalcination temperature from 300, to 500 and then to 550 °C. In addition, the PEC degradation efficiencies using pure NTA photoanode were slightly lower than those of photoanode precalcined at

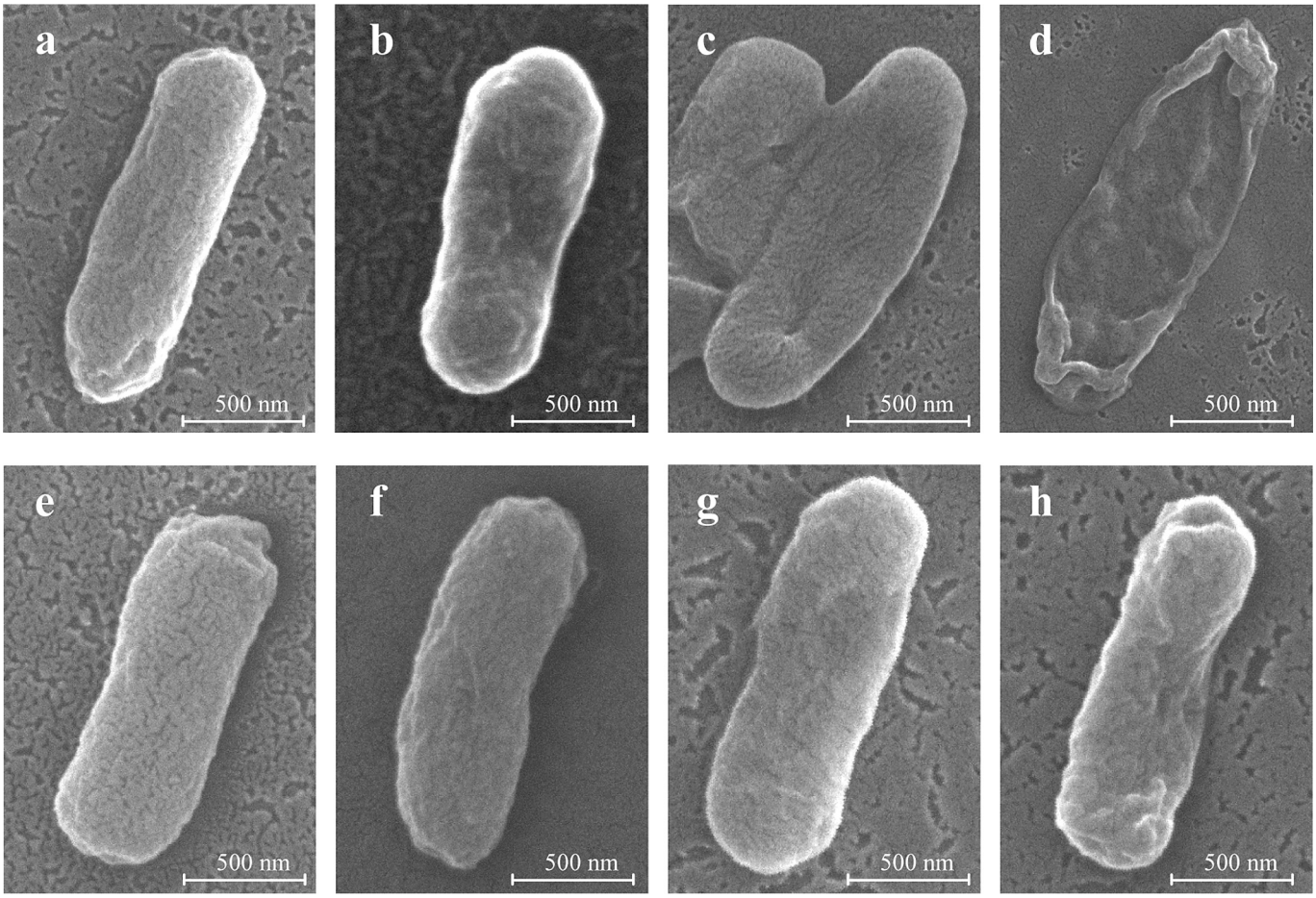

Fig. 4. SEM images of PEC inactivation of *E. coli* in the absence [(a) 0, (b) 30, (c) 60, and (d) 120 min)] and in presence [(e) 0, (f) 30, (g) 60, and (h) 120 min)] of 10 ppm ciprofloxacin.

500 °C. As for using photoanodes prepared at various heating rates to degrade ciprofloxacin (Fig. S10b), the PEC degradation efficiencies of the photoanode obtained with the heating rate of 20 °C min^{-1} were the highest, which was consistent with that for bacterial inactivation. As using photoanodes recalcined at different temperatures after 500 °C precalcination (Fig. S10c), the photoanodes recalcined at 550–650 °C possessed higher photoactivity, which was also consistent with bacterial inactivation results.

3.4. Simultaneous PEC removal of E. coli and ciprofloxacin

From aforementioned results, it can be concluded that *E. coli* or ciprofloxacin can be effectively removed by PEC approach using the optimized photoanode. To further validate the versatility of the resultant photocatalyst to purify water contaminated both with antibiotics and bacteria, the PEC removal of *E. coli* and ciprofloxacin mixture was also carried out under identical condition. First, the mixture solutions of *E. coli* (10^7 cfu mL^{-1}) and ciprofloxacin (0–10 ppm) were only irradiated with UV light (Fig. S11). Similar with the abovementioned results, bacterial population decreased slightly and the ciprofloxacin concentration reduced approximately 33%–39% within 120 min. In addition, the concentrations of bacteria and ciprofloxacin were unchanged after keeping for 4 h under dark, indicating that *E. coli* and ciprofloxacin might be very stable under natural condition.

As using PEC approach, as Fig. 5a shows, all *E. coli* (10^7 cfu mL^{-1}) could be completely inactivated within 45 min in the absence of ciprofloxacin, and the complete inactivation time increased with the increase of ciprofloxacin concentration. For instance, time needed to completely inactivate all bacteria is prolonged from 45 to 150 min in the presence of 0 and 10 ppm ciprofloxacin. This is due to that RSs concentration in PEC system is constant, and extra added organics will compete RSs with bacteria. As such, less RSs will attack bacteria, and subsequently prolong the bacterial inactivation time (Moncayo-Lasso et al., 2012). These results can also be further proved by SEM characterization. As Fig. 4 shows, in the presence of 10 ppm ciprofloxacin, the damage of bacterial cell was not so obvious, and the bacteria still maintained the intact cell structure and rod shape after 60 min treatment as compared with the system without ciprofloxacin. As Fig. 5a shows, the bacterial population decreased only 1.0-log at this time. However, with longer PEC treatment (120 min) in the presence of ciprofloxacin, similar cell damages (Fig. 4h) were observed as the cell treated for 30 min without ciprofloxacin (Fig. 4b).

Meantime, ciprofloxacin removal in the absence and presence of *E. coli* (10^7 cfu mL^{-1}) was also carried out. As Fig. 5b and c shows, although PEC degradation efficiencies of ciprofloxacin increased gradually with the decrease of ciprofloxacin concentration with or without bacteria addition, the degradation process was also delayed with addition of bacteria. Similar results were also observed by other report (Moncayo-Lasso et al., 2012).

4. Conclusions

In sum, using an anodization-precalcination-recalcination approach, a novel TiO_2-based photoanode with a NTA bottom

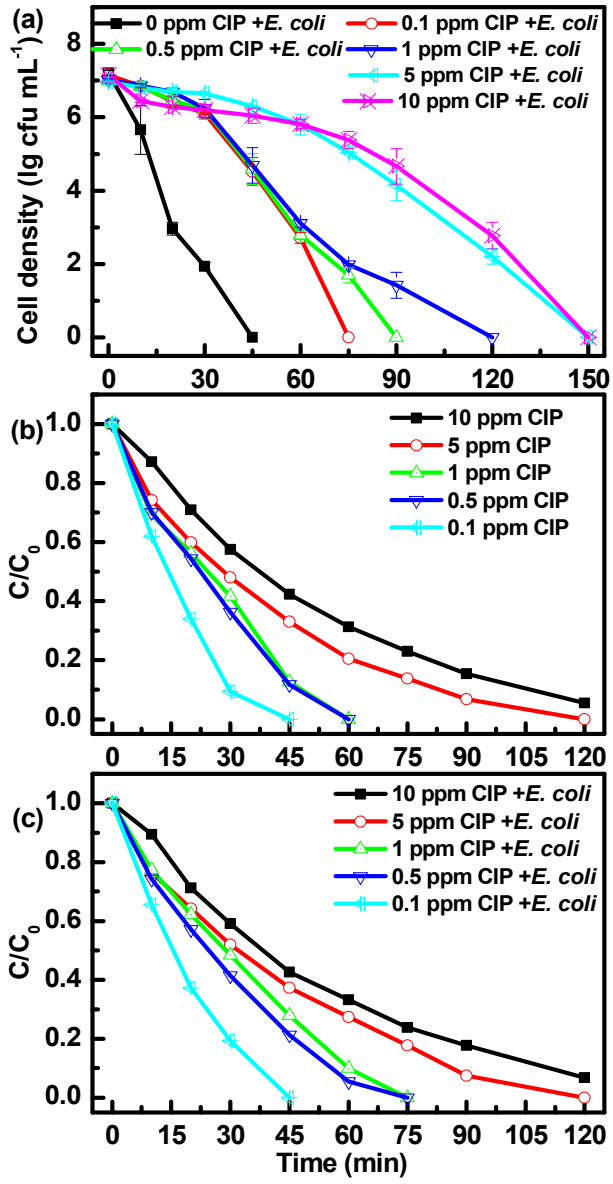

Fig. 5. PEC inactivation of *E. coli* (10^7 cfu mL^{-1}) in the presence of various concentrations of ciprofloxacin (CIP) (a); PEC degradation of various concentrations of ciprofloxacin (CIP) in absence (b) and presence of 10^7 cfu mL^{-1} *E. coli* (c), using the optimized photoanode.

layer covered with exposed high-energy {001} facets top layer was successfully synthesized. In this process, TiO_2 NTA was firstly synthesized on Ti foil by anodization. Then anatase TiO_2 {101} facets at opening ends of NTA directly facing the glass transformed into {001} facets during precalcination as the NTA clamped with two pieces of glasses, and the surface F element in {001} facets was finally removed during appropriate recalcination after removing the covered glasses. Photoelectrocatalytic performance of the resultant photoanodes showed that the optimized TiO_2-based NSC/NTA photoanode possessed excellent PEC activity to remove bacteria, antibiotics as well as mixture of bacteria and antibiotics simultaneously.

Acknowledgments

This work was supported by National Natural Science Funds for Distinguished Young Scholars (41425015); NSFC (41573086 and 41373103); Australian Research Council (ARC) Discovery Project and Research Grant Council, Hong Kong SAR Government (GRF14100115).

Appendix A. Supplementary data

Supplementary data related to this article can be found at http://dx.doi.org/10.1016/j.watres.2016.06.001.

References

Acero, J.L., Benitez, F.J., Real, F.J., Roldan, G., Rodriguez, E., 2013. Chlorination and bromination kinetics of emerging contaminants in aqueous systems. Chem. Eng. J. 219, 43–50.
Alivov, Y., Fan, Z.Y., 2009. A method for fabrication of pyramid-shaped TiO_2 nanoparticles with a high {001} facet percentage. J. Phys. Chem. C 113, 12954–12957.
Almeida, J., Tome, J.P.C., Neves, M.G.P.M.S., Tome, A.C., Cavaleiro, J.A.S., Cunha, A., Costa, L., Faustino, M.A.F., Almeida, A., 2014. Photodynamic inactivation of multidrug-resistant bacteria in hospital wastewaters: influence of residual antibiotics. Photoch. Photobio. Sci. 13, 626–633.
An, T.C., An, J.B., Gao, Y.P., Li, G.Y., Fang, H.S., Song, W.H., 2015. Photocatalytic degradation and mineralization mechanism and toxicity assessment of antivirus drug acyclovir: experimental and theoretical studies. Appl. Catal. B Environ. 164, 279–287.
An, T.C., Chen, J.Y., Nie, X., Li, G.Y., Zhang, H.M., Liu, X.L., Zhao, H.J., 2012. Synthesis of carbon nanotube-anatase TiO_2 sub-micrometer-sized sphere composite photocatalyst for synergistic degradation of gaseous styrene. ACS Appl. Mater. Interfaces 4, 5988–5996.
An, T.C., Liu, J.K., Li, G.Y., Zhang, S.Q., Zhao, H.J., Zeng, X.Y., Sheng, G.Y., Fu, J.M., 2008. Structural and photocatalytic degradation characteristics of hydrothermally treated mesoporous TiO_2. Appl. Catal. A Gen. 350, 237–243.
An, T.C., Sun, H.W., Li, G.Y., Zhao, H.J., Wong, P.K., 2016. Differences in photoelectrocatalytic inactivation processes between E-coli and its isogenic single gene knockoff mutants: destruction of membrane framework or associated proteins? Appl. Catal. B Environ. 188, 360–366.
Baquero, F., Martinez, J.L., Canton, R., 2008. Antibiotics and antibiotic resistance in water environments. Curr. Opin. Biotech. 19 (3), 260–265.
Benkstein, K.D., Kopidakis, N., Van De Lagemaat, J., Frank, A.J., 2003. Influence of the percolation network geometry on electron transport in dye-sensitized titanium dioxide solar cells. J. Phys. Chem. B 107, 7759–7767.
Butterfield, I.M., Christensen, P.A., Curtis, T.P., Gunlazuardi, J., 1997. Water disinfection using an immobilised titanium dioxide film in a photochemical reactor with electric field enhancement. Water Res. 31, 675–677.
Cho, M., Cates, E.L., Kim, J., 2011. Inactivation and surface interactions of MS-2 bacteriophage in a TiO_2 photoelectrocatalytic reactor. Water Res. 45, 2104–2110.
Daghrir, R., Drogui, P., Delegan, N., El Khakani, M.A., 2013. Electrochemical degradation of chlortetracycline using N-doped Ti/TiO_2 photoanode under sunlight irradiations. Water Res. 47, 6801–6810.
de Man, H., van den Berg, H.H.J.L., Leenen, E.J.T.M., Schijven, J.F., Schets, F.M., van der Vliet, J.C., van Knapen, F., Husman, A.M.D., 2014. Quantitative assessment of infection risk from exposure to waterborne pathogens in urban floodwater. Water Res. 48, 90–99.
Dobrowsky, P.H., De Kwaadsteniet, M., Cloete, T.E., Khan, W., 2014. Distribution of indigenous bacterial pathogens and potential pathogens associated with roof-harvested rainwater. Appl. Environ. Microbiol. 80, 2307–2316.
Fletcher, S., 2015. Understanding the contribution of environmental factors in the spread of antimicrobial resistance. Environ. Health Prev. Med. 20, 243–252.
Gao, M.H., An, T.C., Li, G.Y., Nie, X., Yip, H.Y., Zhao, H., Wong, P.K., 2012. Genetic studies of the role of fatty acid and coenzyme A in photocatalytic inactivation of *Escherichia coli*. Water Res. 46, 3951–3957.
Gordon, T.R., Cargnello, M., Paik, T., Mangolini, F., Weber, R.T., Fornasiero, P., Murray, C.B., 2012. Nonaqueous synthesis of TiO_2 nanocrystals using TiF_4 to engineer morphology, oxygen vacancy concentration, and photocatalytic activity. J. Am. Chem. Soc. 134, 6751–6761.
Grimes, C.A., Shankar, K., Basham, J.I., Allam, N.K., Varghese, O.K., Mor, G.K., Feng, X.J., Paulose, M., Seabold, J.A., Choi, K.S., 2009. Recent advances in the use of TiO_2 nanotube and nanowire arrays for oxidative photoelectrochemistry. J. Phys. Chem. C 113, 6327–6359.
Jarosz, M., Syrek, K., Kapusta-Kolodziej, J., Mech, J., Malek, K., Hnida, K., Lojewski, T., Jaskula, M., Sulka, G.D., 2015. Heat treatment effect on crystalline structure and photoelectrochemical properties of anodic TiO_2 nanotube arrays formed in ethylene glycol and glycerol based electrolytes. J. Phys. Chem. C 119, 24182–24191.
Lai, Z.C., Peng, F., Wang, Y., Wang, H.J., Yu, H., Liu, P.R., Zhao, H.J., 2012. Low temperature solvothermal synthesis of anatase TiO_2 single crystals with wholly {100} and {001} faceted surfaces. J. Mater. Chem. 22, 23906–23912.
Li, G.Y., Liu, X.L., An, T.C., Yang, H., Zhang, S.Q., Zhao, H.J., 2015. Photocatalytic and photoelectrocatalytic degradation of small biological compounds at TiO_2 photoanode: a case study of nucleotide bases. Catal. Today 242, 363–371.

Li, G.Y., Liu, X.L., Zhang, H.M., An, T.C., Zhang, S.Q., Carroll, A.R., Zhao, H.J., 2011. In situ photoelectrocatalytic generation of bactericide for instant inactivation and rapid decomposition of Gram-negative bacteria. J. Catal. 277, 88–94.
Li, G.Y., Liu, X.L., Zhang, H.M., Wong, P.K., An, T.C., Zhao, H.J., 2013. Comparative studies of photocatalytic and photoelectrocatalytic inactivation of E. coli in presence of halides. Appl. Catal. B Environ. 140, 225–232.
Liao, Y.L., Zhang, H.W., Que, W.X., Zhong, P., Bai, F.M., Zhong, Z.Y., Wen, Q.Y., Chen, W.H., 2013. Activating the single-crystal TiO_2 nanoparticle film with exposed {001} facets. ACS Appl. Mater. Interfaces 5, 6463–6466.
Liu, C.Y., Fu, D.F., Li, H.H., 2012. Behaviour of multi-component mixtures of tetracyclines when degraded by photoelectrocatalytic and electrocatalytic technologies. Environ. Technol. 33, 791–799.
Liu, G., Yang, H.G., Wang, X.W., Cheng, L.N., Lu, H.F., Wang, L.Z., Lu, G.Q., Cheng, H.M., 2009a. Enhanced photoactivity of oxygen-deficient anatase TiO_2 sheets with dominant {001} facets. J. Phys. Chem. C 113, 21784–21788.
Liu, G., Yang, H.G., Wang, X.W., Cheng, L.N., Pan, J., Lu, G.Q., Cheng, H.M., 2009b. Visible light responsive nitrogen doped anatase TiO_2 sheets with dominant {001} facets derived from TiN. J. Am. Chem. Soc. 131, 12868–12869.
Liu, J.K., An, T.C., Li, G.Y., Bao, N.Z., Sheng, G.Y., Fu, J.M., 2009c. Preparation and characterization of highly active mesoporous TiO_2 photocatalysts by hydrothermal synthesis under weak acid conditions. Micropor. Mesopor. Mat. 124, 197–203.
Liu, M., Piao, L.Y., Zhao, L., Ju, S.T., Yan, Z.J., He, T., Zhou, C.L., Wang, W.J., 2010. Anatase TiO_2 single crystals with exposed {001} and {110} facets: facile synthesis and enhanced photocatalysis. Chem. Commun. 46, 1664–1666.
Marugan, J., van Grieken, R., Pablos, C., Sordo, C., 2010. Analogies and differences between photocatalytic oxidation of chemicals and photocatalytic inactivation of microorganisms. Water Res. 44, 789–796.
Mather, A.E., 2014. Antibiotics and collateral damage. Science 344, 472–473.
Michael, I., Rizzo, L., McArdell, C.S., Manaia, C.M., Merlin, C., Schwartz, T., Dagot, C., Fatta-Kassinos, D., 2013. Urban wastewater treatment plants as hotspots for the release of antibiotics in the environment: a review. Water Res. 47, 957–995.
Moncayo-Lasso, A., Mora-Arismendi, L.E., Rengifo-Herrera, J.A., Sanabria, J., Benitez, N., Pulgarin, C., 2012. The detrimental influence of bacteria (*E. coli, Shigella* and *Salmonella*) on the degradation of organic compounds (and vice versa) in TiO_2 photocatalysis and near-neutral photo-Fenton processes under simulated solar light. Photochem. Photobiol. Sci. 11, 821–827.
Munir, M., Wong, K., Xagoraraki, I., 2011. Release of antibiotic resistant bacteria and genes in the effluent and biosolids of five wastewater utilities in Michigan. Water Res. 45, 681–693.
Na, G.S., Zhang, W.R., Zhou, S.Y., Gao, H., Lu, Z.H., Wu, X., Li, R.J., Qiu, L.N., Cai, Y.Q., Yao, Z.W., 2014. Sulfonamide antibiotics in the Northern Yellow Sea are related to resistant bacteria: implications for antibiotic resistance genes. Mar. Pollut. Bull. 84, 70–75.
Nie, X., Chen, J.Y., Li, G.Y., Shi, H.X., Zhao, H.J., Wong, P.K., An, T.C., 2013. Synthesis and characterization of TiO_2 nanotube photoanode and its application in photoelectrocatalytic degradation of model environmental pharmaceuticals. J. Chem. Technol. Biotechnol. 88, 1488–1497.
Nie, X., Li, G.Y., Gao, M.H., Sun, H.W., Liu, X.L., Zhao, H.J., Wong, P.K., An, T.C., 2014a. Comparative study on the photoelectrocatalytic inactivation of Escherichia coli K-12 and its mutant Escherichia coli BW25113 using TiO2 nanotubes as a photoanode. Appl. Catal. B Environ. 147, 562–570.
Nie, X., Li, G.Y., Wong, P.K., Zhao, H.J., An, T.C., 2014b. Synthesis and characterization of N-doped carbonaceous/TiO_2 composite photoanodes for visible-light photoelectrocatalytic inactivation of *Escherichia coil* K-12. Catal. Today 230, 67–73.
Paulose, M., Shankar, K., Varghese, O.K., Mor, G.K., Grimes, C.A., 2006. Application of highly-ordered TiO_2 nanotube-arrays in heterojunction dye-sensitized solar cells. J. Phys. D. Appl. Phys. 39, 2498–2503.
Rizzo, L., Manaia, C., Merlin, C., Schwartz, T., Dagot, C., Ploy, M.C., Michael, I., Fatta-Kassinos, D., 2013. Urban wastewater treatment plants as hotspots for antibiotic resistant bacteria and genes spread into the environment: a review. Sci. Total Environ. 447, 345–360.
Schmuki, P., Roy, P., Berger, S., 2011. TiO2 nanotubes: synthesis and applications. Angew. Chem. Int. Ed. 50, 2904–2939.
Selloni, A., 2008. Crystal growth - anatase shows its reactive side. Nat. Mater. 7, 613–615.
Stefanov, B.I., Niklasson, G.A., Granqvist, C.G., Osterlund, L., 2016. Gas-phase photocatalytic activity of sputter-deposited anatase TiO_2 films: effect of {001} preferential orientation, surface temperature and humidity. J. Catal. 335, 187–196.
Sun, H.W., Li, G.Y., An, T.C., Zhao, H.J., Wong, P.K., 2016. Unveiling the photoelectrocatalytic inactivation mechanism of *Escherichia coli*: convincing evidence from responses of parent and anti-oxidation single gene knockout mutants. Water Res. 88, 135–143.
Sun, H.W., Li, G.Y., Nie, X., Shi, H.X., Wong, P.K., Zhao, H.J., An, T.C., 2014. Systematic approach to in-depth understanding of photoelectrocatalytic bacterial inactivation mechanisms by tracking the decomposed building blocks. Environ. Sci. Technol. 48, 9412–9419.
Yang, H.G., Sun, C.H., Qiao, S.Z., Zou, J., Liu, G., Smith, S.C., Cheng, H.M., Lu, G.Q., 2008. Anatase TiO_2 single crystals with a large percentage of reactive facets. Nature 453, 638–641.
Yang, W.G., Li, J.M., Wang, Y.L., Zhu, F., Shi, W.M., Wan, F.R., Xu, D.S., 2011. A facile synthesis of anatase TiO2 nanosheets-based hierarchical spheres with over 90% {001} facets for dye-sensitized solar cells. Chem. Commun. 47, 1809–1811.
Yu, H., Zhang, S.Q., Zhao, H.J., Xue, B.F., Liu, P.R., Will, G., 2009. High-performance TiO_2 photoanode with an efficient electron transport network for dye-sensitized solar cells. J. Phys. Chem. C 113, 16277–16282.
Yu, J.G., Wang, B., 2010. Effect of calcination temperature on morphology and photoelectrochemical properties of anodized titanium dioxide nanotube arrays. Appl. Catal. B Environ. 94, 295–302.
Zhang, H., Zhao, H., Zhang, S., Quan, X., 2008. Photoelectrochemical manifestation of photoelectron transport properties of vertically aligned nanotubular TiO_2 photoanodes. ChemPhysChem 9, 117–123.
Zhang, H.M., Han, Y.H., Liu, X.L., Liu, P.R., Yu, H., Zhang, S.Q., Yao, X.D., Zhao, H.J., 2010. Anatase TiO2 microspheres with exposed mirror-like plane {001} facets for high performance dye-sensitized solar cells (DSSCs). Chem. Commun. 46, 8395–8397.
Zhang, H.M., Liu, P.R., Li, F., Liu, H.W., Wang, Y., Zhang, S.Q., Guo, M.X., Cheng, H.M., Zhao, H.J., 2011a. Facile fabrication of anatase TiO_2 microspheres on solid substrates and surface crystal facet transformation from {001} to {101}. Chem. Eur. J. 17, 5949–5957.
Zhang, H.M., Wang, Y., Liu, P.R., Han, Y.H., Yao, X.D., Zou, J., Cheng, H.M., Zhao, H.J., 2011b. Anatase TiO_2 crystal facet growth: mechanistic role of hydrofluoric acid and photoelectrocatalytic activity. ACS Appl. Mater. Interfaces 3, 2472–2478.
Zhao, H.J., Jiang, D.L., Zhang, S.Q., Catterall, K., John, R., 2004. Development of a direct photoelectrochemical method for determination of chemical oxygen demand. Anal. Chem. 76, 155–160.
Zhu, K., Neale, N.R., Miedaner, A., Frank, A.J., 2007. Enhanced charge-collection efficiencies and light scattering in dye-sensitized solar cells using oriented TiO_2 nanotubes arrays. Nano Lett. 7, 69–74.